Heterogeneous Catalysis Hot Paper

How to cite: *Angew. Chem. Int. Ed.* **2020**, *59*, 11647–11652
International Edition: doi.org/10.1002/anie.202004966
German Edition: doi.org/10.1002/ange.202004966

Adsorption Site Regulation to Guide Atomic Design of Ni–Ga Catalysts for Acetylene Semi-Hydrogenation

Yueqiang Cao[+], Hao Zhang[+], Shufang Ji, Zhijun Sui, Zheng Jiang, Dingsheng Wang, Francisco Zaera, Xinggui Zhou, Xuezhi Duan,* and Yadong Li*

Abstract: *Atomic regulation of metal catalysts has emerged as an intriguing yet challenging strategy to boost product selectivity. Here, we report a density functional theory-guided atomic design strategy for the fabrication of a NiGa intermetallic catalyst with completely isolated Ni sites to optimize acetylene semi-hydrogenation processes. Such Ni sites show not only preferential acetylene π-adsorption, but also enhanced ethylene desorption. The characteristics of the Ni sites are confirmed by multiple characterization techniques, including aberration-corrected high-resolution scanning transmission electron microscopy and X-ray absorption spectrometry measurements. The superior performance is also confirmed experimentally against a Ni_5Ga_3 intermetallic catalyst with partially isolated Ni sites and against a Ni catalyst with multi-atomic ensemble Ni sites. Accordingly, the NiGa intermetallic catalyst with the completely isolated Ni sites shows significantly enhanced selectivity to ethylene and suppressed coke formation.*

Introduction

Catalytic acetylene semi-hydrogenation to ethylene by restraining its full-hydrogenation and oligomerization has long been a crucial yet challenging step for the cost-effective and environmentally benign removal of trace acetylene impurities in the polyethylene industry.[1] The most common industrially used catalyst is based on Pd modified with Ag. Theoretical predictions of density functional theory (DFT) scaling analysis across the alloys of late 3d transition metals together with experimental verification by Nørskov and coworkers have shown non-noble Ni–Zn alloy combinations as a substitution of noble Pd-based catalysts.[2] Such optimal substitute, exhibiting relatively high selectivity to ethylene, benefits from a compromise between strong acetylene adsorption and weak ethylene adsorption. The principle behind this phenomenon is to understand how the processed molecules match the active sites of the catalyst at an atomic level,[3] but it remains elusive and is a field of emerging research for achieving the atomic design and development of alternative catalysts for acetylene semi-hydrogenation.

As a potential alternative, the rational design and atomic regulation of Ni-based catalysts are critical to precisely control the adsorption/desorption properties in relation to the catalytic activity/selectivity.[4] Generally, the reported pure Ni catalysts not only exhibited very low selectivity for ethylene and poor stability, due to the strong acetylene adsorption based on theoretical results,[5] but also co-existed in various adsorption configurations, i.e., π- and σ-adsorptions, based on C_2H_4-TPD studies.[6] Importantly, dominantly existing π-adsorption and weakened σ-adsorption on the NiIn and Ni_3Ga catalysts, respectively, were observed to exhibit relatively high selectivity for ethylene.[4a,6] To rationally design and regulate Ni–M catalysts, it requires DFT calculations to realize the intrinsically Ni sites-dependent adsorption–desorption behaviors with the aim to determine unique configuration of Ni sites for catalytic acetylene semi-hydrogenation. Additionally, considering remarkable structure sensitivity of metal-catalyzed acetylene hydrogenation,[7] a controllable synthesis strategy needs to be developed, which would ensure negligible changes in the Ni–M particle sizes and atomically ordered arrangement of Ni and M elements when adding other metal components (e.g., Ga and In).

To address these urgent yet unresolved issues and provide theoretical basis for the atomic design of highly selective Ni catalysts for acetylene semi-hydrogenation, we employed DFT calculations to explore the adsorption/desorption and hydrogenation properties at different typed Ni sites, i.e., completely isolated, partially separated and contiguous Ni sites. The completely isolated Ni sites were found to not only facilitate the preferential π-adsorption of acetylene reactant,

[*] Dr. Y. Cao,[+] Prof. Z. Sui, Prof. X. Zhou, Prof. X. Duan
State Key Laboratory of Chemical Engineering, School of Chemical Engineering, East China University of Science and Technology
Shanghai 200237 (China)
E-mail: xzduan@ecust.edu.cn
H. Zhang,[+] Prof. Z. Jiang
Shanghai Institute of Applied Physics, Chinese Academy of Science
Shanghai 201800 (China)
Dr. S. Ji, Prof. D. Wang, Prof. Y. Li
Department of Chemistry, Tsinghua University
Beijing 100084 (China)
E-mail: wangdingsheng@mail.tsinghua.edu.cn
Prof. F. Zaera
Department of Chemistry and UCR Center for Catalysis, University of California, Riverside, CA 92521 (USA)
H. Zhang[+]
University of Chinese Academy of Sciences
Beijing 100049 (China)
Prof. Z. Jiang
Shanghai Synchrotron Radiation Facility, Zhangjiang Lab, Shanghai Advanced Research Institute, Chinese Academy of Science
Shanghai 201210 (China)
[+] These authors contributed equally to this work.
Supporting information and the ORCID identification number(s) for the author(s) of this article can be found under https://doi.org/10.1002/anie.202004966.

but also promote the desorption of targeted ethylene product. Further controllable synthesis of NiGa, Ni_5Ga_3 and Ni with the accordingly different Ni sites but similar particle sizes confirmed that atomically regulating the Ni sites to the completely isolated ones is an effective strategy to boost the selectivity for ethylene and suppress coke formation.

Results and Discussion

DFT calculations were first performed to probe the structural, electronic and catalytic properties of two representative Ni–Ga intermetallic catalysts, i.e., NiGa with completely isolated Ni sites and Ni_5Ga_3 with partially separated Ni sites (see Figure S1 in the Supporting Information), according to the Ni–Ga binary phase diagram.[8] Simulated XRD patterns of Ni, Ni_5Ga_3 and NiGa (Figure 1a) together with the Wulff construction results[9] indicate (111), (221) and (110) as their thermodynamically stable and mostly exposed surfaces. Local density of states (i.e., LDOS) projected onto the Ni sites in Figure 1b show that the higher ratio of Ga/Ni corresponds to the lower d-band center of Ni away from the Fermi level and transfers more electrons to the Ni sites (Figure S2). Figure 1c and d show the configurations and energies of the most stable acetylene adsorption on these surfaces, respectively. Clearly, regulating the Ni sites to the completely isolated Ni ones by Ga gives rise to preferential π-adsorption of acetylene, and the adsorption energies decrease in order of Ni(111) > Ni_5Ga_3(221) > NiGa(110), as revealed by both the less elongated bond length and transferred charges from Ni sites to the adsorbed acetylene (Figure 1d).

The competition between hydrogenation and desorption of the targeted ethylene species, which determines the selectivity to ethylene[3b,5a] over these different Ni-based surfaces was further investigated. As expected in Figure 1d and Figure S3, the completely isolated Ni sites on NiGa(110) show preferential ethylene π-adsorption and significantly decreased adsorption energy, which would be favorable for ethylene desorption. To quantitatively compare ethylene desorption versus hydrogenation, their Gibbs free energies at the reaction temperature of 150 °C were calculated; the optimized adsorption configurations of the involved species are summarized in Figure S4. As can be seen in Figure 1e, Ni(111) shows the highest ethylene desorption free energy and the lowest hydrogenation free energy barrier, which is consistent with the experimentally observed low selectivity for ethylene.[4b,10] Meanwhile, Ni(111) with the contiguous Ni sites and Ni_5Ga_3(221) with partially separated Ni sites, both of which contain ensemble Ni sites, show higher ethylene desorption free energy than hydrogenation free energy barrier, while NiGa(110) with completely isolated Ni sites shows much lower free energy barrier for ethylene desorption than for hydrogenation. This strongly indicates that the completely isolated Ni sites are much more selective to yield the targeted ethylene product. Notably, NiGa(110) unexpectedly shows a lower hydrogenation barrier than Ni_5Ga_3(221), which is most likely due to unique geometric effects. Furthermore, for the completely isolated Ni sites on the NiGa catalyst, the step-like NiGa(221) also shows significantly enhanced ethylene desorption, while for the ensemble Ni sites over the Ni_5Ga_3 catalyst, the step-like Ni_5Ga_3(110) exhibits favorable ethylene hydrogenation in Figure S5. All of these results highlight the crucial importance of regulating the ensemble Ni sites to the completely isolated ones for the semi-hydrogenation process.

To confirm the theoretical predictions, further controllable synthesis of NiGa, Ni_5Ga_3 and Ni catalysts was carried out via a co-precipitation method to form layered double hydroxides (LDHs) followed by H_2 reduction, by taking advantage of the unique LDH structure, i.e., ordered and uniform distribution of Ni and Ga cations in the brucite layer, for the formation of uniform Ni–Ga intermetallic catalysts.[4d,11] X-ray diffraction (XRD), scanning electron microscopy, energy-dispersive X-ray spectroscopy (EDS) mapping and thermogravimetric analysis (Figures S6–S9) confirm the formation of LDHs. Transmission electron microscopy (TEM) and high-angle annular dark-field scanning transmission electron microscopy (HAADF-STEM) images as well as the corresponding particle size distributions shown in Figure S10 and Figure 2a–c exhibit similar particle sizes over the three catalysts, which allows us to understand the underlying effects of Ni sites under excluding the size effects on the reaction. Further combining with single particle EDS line scanning and mapping technique, the two Ni–Ga catalysts compared to the Ni catalyst show uniform distributions of Ni and Ga atoms within the nanoparticles in Figure 2d. XRD measurements in Figure S11 indicate that the Ni species of these three reduced catalysts from each LDHs most likely exist in the forms of Ni metallic phase as well as Ni_5Ga_3 and NiGa intermetallic phases, respectively. These are further supported by the determined lattice spacings and/or interplanar angle using high-resolution TEM (HRTEM) and fast Fourier transform (FFT) techniques in Figure 2e–g. There-

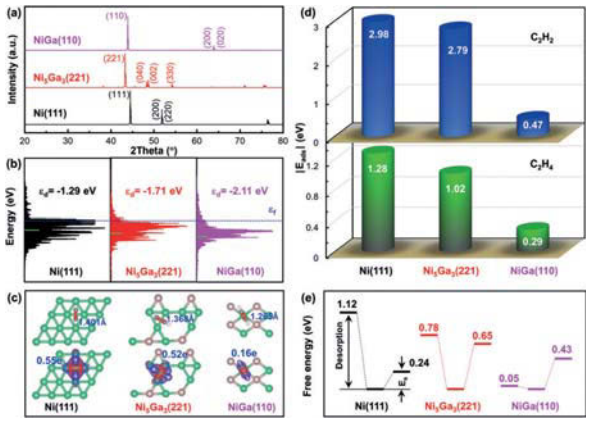

Figure 1. a) Simulated XRD patterns of Ni, Ni_5Ga_3 and NiGa, where the crystal planes were indexed according to their standard patterns of JCPDS No. 04-0850, JCPDS No. 43-1376 and JCPDS No. 65-6413. b) LDOS analysis of Ni(111), Ni_5Ga_3(221) and NiGa(110) surfaces. c) Adsorption configurations of acetylene and corresponding charge density distributions as well as d) adsorption energies of acetylene and ethylene. e) Gibbs free energies for the ethylene desorption versus hydrogenation over Ni(111), Ni_5Ga_3(221) and NiGa(110) surfaces at 150 °C.

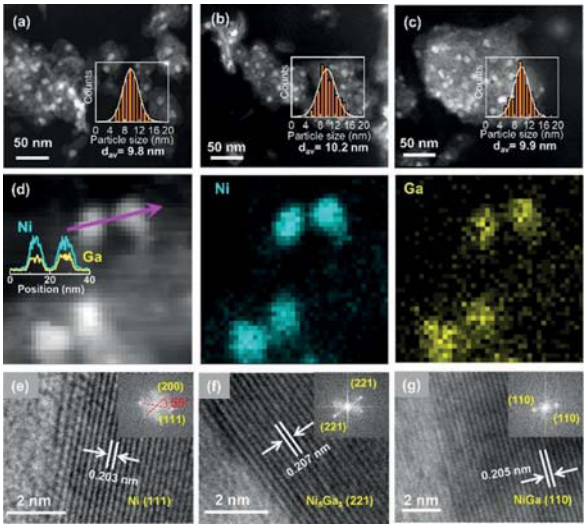

Figure 2. HAADF-STEM images a) Ni, b) Ni_5Ga_3 and c) NiGa catalysts. d) HAADF-STEM EDS mapping of Ni_5Ga_3 with the EDS line-scanning profile shown in the inset along the pink arrow. HRTEM images of e) Ni, f) Ni_5Ga_3 and g) NiGa catalysts and the corresponding FFT patterns shown in the insets.

fore, fabricating the LDHs followed by H_2 reduction is found to be an effective strategy for obtaining Ni–Ga intermetallic catalysts.

To gain more microstructural insights into the fabricated Ni–Ga intermetallic catalysts, we resort to the spherical aberration corrected HAADF-STEM (AC-HAADF-STEM) technique for the Ni_5Ga_3 and NiGa catalysts. Figure 3a shows the typical AC-HAADF-STEM image of Ni_5Ga_3 catalyst. The integrated pixel intensity profile was derived from the line marked by the yellow arrow in Figure 3a, and the results are shown in Figure 3b. The averaged spacing is calculated to be 0.19 nm, which is assigned to the (221) plane of Ni_5Ga_3 intermetallic phase, and the lattice spacing of 0.21 nm is assigned to its (002) plane using the similar method. According to the enlarged view of the atomic distribution in Figure 3c, the corresponding FFT analysis was conducted to determine the zone axis. As obtained in Figure 3d, the ideal crystal structural model of Ni_5Ga_3 intermetallic along with the $[\bar{1}10]$ zone axis is well consistent with the observed atomic arrangement in Figure 3c. Similarly, the lattice spacing of 0.17 nm is assigned to the (111) of NiGa intermetallic phase in Figure 3e and f. The FFT analysis for the enlarged view in Figure 3g reveals the characteristic reflection of the $[\bar{1}\bar{1}2]$ zone axis (Figure 3h). The ideal crystal structural model of NiGa intermetallic along with such zone axis agrees well with the observed atomic arrangement in Figure 3g. These results clearly demonstrate that facilely regulating the Ga/Ni ratio to synthesize well-defined Ni–Ga intermetallic catalysts by the H_2 reduction of LDHs can achieve the precise atomic arrangement and design of Ni sites at the atomic level.

X-ray absorption spectra, including Fourier transformed and Wavelet transformed extended X-ray absorption fine structure (FT-EXAFS and WT-EXAFS) at both Ni and Ga K-edge, were further conducted to understand the local environments of Ni sites over the three catalysts, and the results are shown in Figure S12–S16. As demonstrated by the WT-EXAFS contour plots of Ni and Ga K-edges in Figure 4a–e, the k-axis location of the scattering center shifts to lower value with the increase of Ga/Ni ratio. By combining with the above results, the introduction of Ga is suggested to increase the atomic disorder of Ni and eventually yield the targeted complete isolation of Ni sites over the NiGa catalyst. Meanwhile, the EXAFS oscillations of the Ni-Ga intermetallic catalysts, i.e., Ni_5Ga_3 and NiGa catalysts, exhibit shorter periods and smaller amplitudes compared to the Ni foil and Ni catalyst (in Figure 4f), indicating the longer Ni–Ga(Ni) distances and lower Ni coordination environment in the Ni–Ga intermetallic catalysts.[12] The curve fittings for the experimental results in R space of Ni and Ga K-edge EXAFS were then performed to quantitatively analyze local environ-

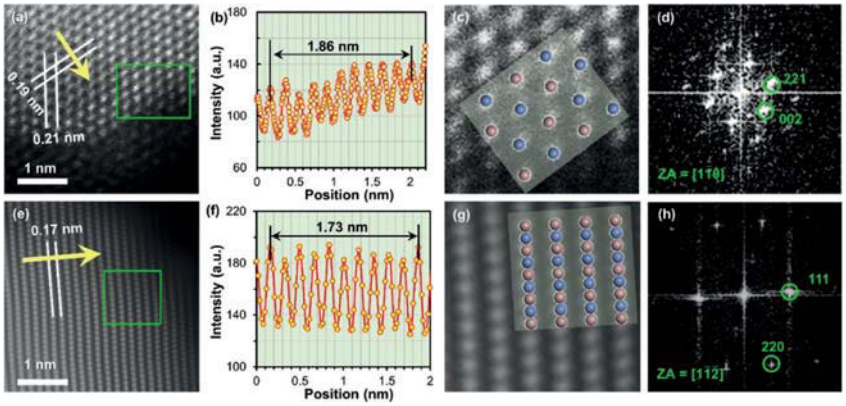

Figure 3. a) AC-HAADF-STEM image of Ni_5Ga_3 catalyst. b) Line intensity profile corresponding to the yellow arrow in (a). c) An enlarged view of the area marked by green rectangle in (a) and the corresponding crystal model along with the $[\bar{1}10]$ zones. d) The fast Fourier transform (FFT) pattern of Ni_5Ga_3 catalyst. e) AC-HAADF-STEM image of NiGa catalyst. f) Line intensity profile corresponding to the yellow arrow in (e). g) An enlarged view of the area marked by the green rectangle in (e) and the corresponding crystal model along with the $[\bar{1}\bar{1}2]$ zones. h) The fast Fourier transform (FFT) pattern of NiGa catalyst.

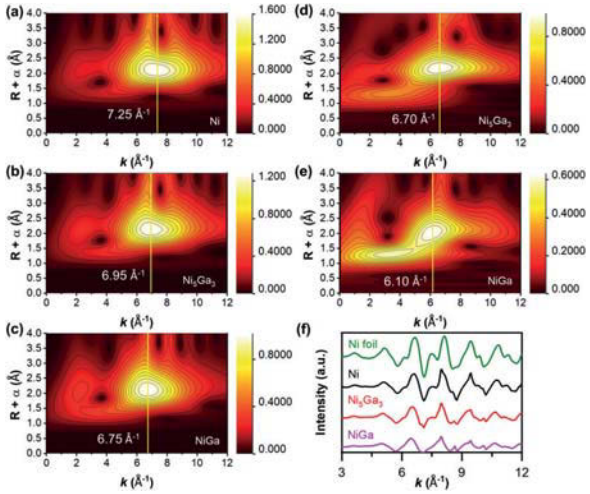

Figure 4. WT-EXAFS of Ni K-edge signal for a) Ni, b) Ni_5Ga_3 and c) NiGa catalysts. WT-EXAFS Ga K-edge signal of d) Ni_5Ga_3 and e) NiGa catalysts. f) EXAFS oscillation functions at the Ni K-edge of Ni foil, Ni, Ni_5Ga_3 and NiGa catalysts.

ment differences among these catalysts, and the results are listed in Table S1. According to the quantitatively fitted results, the $N_{Ni\text{-}Ni}/N_{Ni\text{-}Ga}$ ratio decreases with the Ga/Ni ratio, and eventually the coordination number (CN) of first nearest Ni–Ni bond reduces to 0 for the NiGa catalyst. This strongly demonstrates the absence of Ni–Ni bond, i.e., the complete isolation of Ni sites by Ga, in the NiGa catalyst.

The three fabricated Ni catalysts with the similar metal particle sizes but significantly different atomic arrangements and local environments of Ni sites were comparatively studied for acetylene hydrogenation in the absence of ethylene. As clearly observed in Figure 5a, the Ni and Ni_5Ga_3 catalysts with the ensemble Ni sites show higher activity but much lower selectivity to ethylene especially in the range of 100–260 °C. However, the NiGa catalyst with the completely isolated Ni sites gives rise to the relatively lower activity but much higher selectivity to ethylene. This strongly indicates that regulating the Ni sites up to the complete isolation is a very effective way for remarkably enhancing the selectivity to the targeted ethylene product.

It can be also seen in Figure 5a that for the ensemble Ni sites, the Ni and Ni_5Ga_3 catalysts show a reverse volcano-shaped selectivity to ethylene with the temperature, which could be due to a trade-off between the acetylene over-hydrogenation to ethane and ethylene desorption as the temperature increases.[10,13] In particular, in the high-temperature range, both the Ni and Ni_5Ga_3 catalysts show the same acetylene conversions, but increased selectivities to ethylene with the temperature. To understand this issue, effects of the temperature on the free energies for the ethylene desorption and hydrogenation were comparatively studied. As shown in Figure S17, the temperature remarkably decreases the ethylene desorption free energy, but slightly affects the ethylene hydrogenation free energy barrier. This could provide a rational interpretation for the increased selectivity to ethylene at the relatively high temperature. More interestingly, for the completely isolated Ni sites, the NiGa catalyst shows the almost unchanged selectivity to ethylene, i.e., ca. 82 %, in the whole tested temperature range. These results suggest regulating the Ni sites to the complete isolation as a promising strategy for acetylene semi-hydrogenation.

TPD measurements were further conducted to probe the effects of the different Ni sites over the above three catalysts on the adsorption of acetylene reactant and desorption of targeted ethylene product. As obviously seen in Figure 5b, the Ni and Ni_5Ga_3 catalysts exhibit three legible desorption peaks. Further combining with the results of DFT calculations in Figure S18, the former two peaks (i.e., Peak I and Peak II) at the lower temperatures could be ascribed to the weakly adsorbed C_2H_2 on the support[14] and the weak π-adsorption of C_2H_2, while the Peak III at the higher temperature for the strong σ-adsorption of C_2H_2. In contrast, there is one broad peak at the lower temperature over the NiGa catalyst with the completely isolated Ni sites, but almost lack of high-temperature peak ascribed to the strong σ-adsorption of C_2H_2. These are supported by the only identified weak π-adsorption of C_2H_2 over the NiGa catalyst in Figure S18. Meanwhile, the observed downshifts of C_2H_2 desorption temperature with the

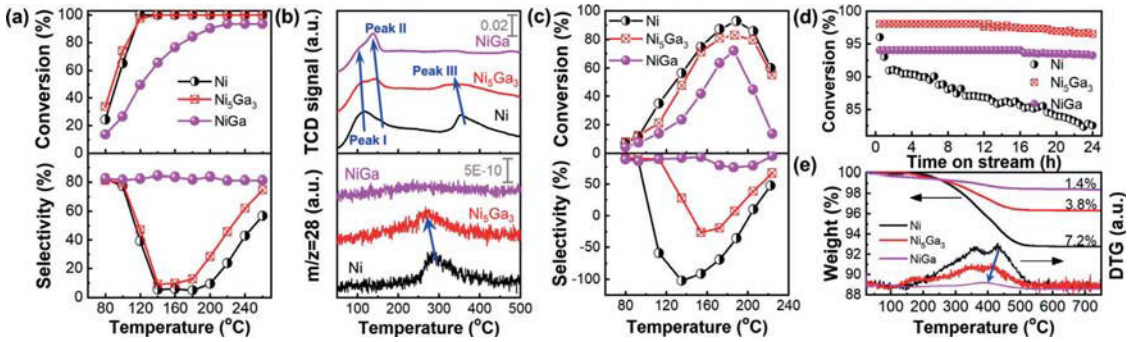

Figure 5. a) Acetylene conversion and ethylene selectivity as a function of reaction temperature for acetylene hydrogenation in the absence of ethylene, b) C_2H_2-TPD (upper) and C_2H_4-TPD (bottom) profiles, c) acetylene conversion and ethylene selectivity as a function of reaction temperature in the presence of ethylene, and d) acetylene conversion as a function of time on stream at 190 °C over the Ni, Ni_5Ga_3 and NiGa catalysts. e) TGA profiles of the used Ni, Ni_5Ga_3 and NiGa catalysts.

Ga/Ni ratio is mainly ascribed to the changed Ni adsorption sites and more electron-rich Ni sites as the introduction of Ga (Figure S19 and S20). It is also observed in Figure 5b that the completely isolated Ni sites over the NiGa catalyst compared to the Ni and Ni_5Ga_3 catalysts give rise to remarkably enhanced desorption of C_2H_4. These results would provide a rational interpretation that the changed adsorption configuration of acetylene reactant and enhanced desorption of targeted ethylene products account for the much higher selectivity to ethylene over the NiGa catalyst.

Considering that practical catalytic system contains excess ethylene, the above three catalysts were also tested for the hydrogenation of acetylene in the presence of excess ethylene. As expected in Figure 5c, in the presence of excess ethylene, the NiGa catalyst with the complete isolation of Ni sites compared the other two catalysts still exhibits much higher and slightly changed selectivity to ethylene in the tested temperature range of 80–220 °C. Meanwhile, as the temperature increases, the acetylene conversions over all these catalysts first increase and then decrease when the temperature is higher than 190 °C. This change is reversible in Figure S21, where the conversion of acetylene can be maintained when the reaction temperature is back to 190 °C, i.e., there are no severe catalyst deactivation. Therefore, the observed low activity in the higher temperature regime is ascribed to the trade-off between the acetylene hydrogenation and its desorption with the temperature rather than the result of an irreversible deactivation of the catalysts.[13b–d]

In addition, the introduction of Ga is shown to not only remarkably enhance the catalytic stabilities in Figure 5d, but also significantly decrease the amount and carbon content of green oil based on the TGA results of the used three catalysts in Figure 5e. It is noted that at the late stage of catalytic process in Figure 5d, the NiGa catalyst shows slightly decreased acetylene conversions. TEM measurements of the used NiGa catalyst in Figure S22 show no obvious agglomeration of intermetallic particles compared to the fresh catalyst. It is therefore suggested that the slightly decreased activity at the reaction late stage mainly arises from the formation and accumulation of green oil, which possibly blocks some Ni active sites. All the above results demonstrate that regulating the Ni sites to the complete isolation is a promising strategy for the positive geometric effects on the acetylene semi-hydrogenation, which gives rise to simultaneously enhanced selectivity to the targeted ethylene product and catalyst stability with the anti-coking to form much less undesirable green oil. Notably, for different catalytic systems, the optimal Ni/Ga ratio is different due to different reaction characteristics, such as the Ni_5Ga_3 and Ni_3Ga intermetallic catalysts with the better performances for the thermo-/electro-chemical conversion of CO_2 and the phenylacetylene semi-hydrogenation, respectively.[4d,15] Future studies are advocated by a combination of DFT calculations with advanced characterization techniques to obtain the mechanistic basis for the underlying relations of the Ni–Ga catalyst geometric/electronic structures with these reaction characteristics, aiming to guide the catalyst rational design and optimization.

Conclusion

In summary, we have demonstrated a DFT-guided atomic design of Ni–Ga catalysts and regulating the Ni sites to the completely isolated ones as an effective strategy for the superior acetylene semi-hydrogenation. The completely isolated Ni sites have exhibited the targeted π-adsorption of acetylene and enhanced desorption of ethylene. The theoretical predictions have been validated by experimental observations of the highly selective and stable NiGa intermetallic catalyst against the Ni_5Ga_3 and Ni catalysts with the ensemble Ni sites. These results are valuable for rational design and manipulation of highly selective yet stable catalysts by atomically regulating the metal sites.

Acknowledgements

This work was financially supported by the Natural Science Foundation of China (21922803 and 21776077), the Natural Science Foundation of Shanghai (17ZR1407300), the Program for Professor of Special Appointment (Eastern Scholar) at Shanghai Institutions of Higher Learning, the Shanghai Rising-Star Program (17QA1401200), the Fundamental Research Funds for the Central Universities (222201718003) and the Open Project of State Key Laboratory of Chemical Engineering (SKL-Che-15C03). F.Z. acknowledges funding from the US National Science Foundation (CHE-1953843). We thank the BL14W1 XAFS beamline of Shanghai Synchrotron Radiation Facility (SSRF) for providing beamtime.

Conflict of interest

The authors declare no conflict of interest.

Keywords: acetylene · heterogeneous catalysis · Ni–Ga intermetallic catalyst · semi-hydrogenation · site regulation

[1] a) A. Borodziński, G. C. Bond, *Catal. Rev.* **2006**, *48*, 91–144; b) J. Osswald, K. Kovnir, M. Armbrüster, R. Giedigkeit, R. E. Jentoft, U. Wild, Y. Grin, R. Schlögl, *J. Catal.* **2008**, *258*, 219–227; c) L. Ding, H. Yi, W. Zhang, R. You, T. Cao, J. Yang, J. Lu, W. Huang, *ACS Catal.* **2016**, *6*, 3700–3707; d) G. X. Pei, X. Y. Liu, X. Yang, L. Zhang, A. Wang, L. Li, H. Wang, X. Wang, T. Zhang, *ACS Catal.* **2017**, *7*, 1491–1500; e) M. Armbrüster, K. Kovnir, M. Behrens, D. Teschner, Y. Grin, R. Schlögl, *J. Am. Chem. Soc.* **2010**, *132*, 14745–14747; f) L. Shao, W. Zhang, M. Armbrüster, D. Teschner, F. Girgsdies, B. Zhang, O. Timpe, M. Friedrich, R. Schlögl, D. S. Su, *Angew. Chem. Int. Ed.* **2011**, *50*, 10231–10235; *Angew. Chem.* **2011**, *123*, 10414–10418.

[2] F. Studt, F. Abild-Pedersen, T. Bligaard, R. Z. Sørensen, C. H. Christensen, J. K. Nørskov, *Science* **2008**, *320*, 1320–1322.

[3] a) H. Zhou, X. Yang, L. Li, X. Liu, Y. Huang, X. Pan, A. Wang, J. Li, T. Zhang, *ACS Catal.* **2016**, *6*, 1054–1061; b) Q. Feng, S. Zhao, Y. Wang, J. Dong, W. Chen, D. He, D. Wang, J. Yang, Y. Zhu, H. Zhu, L. Gu, Z. Li, Y. Liu, R. Yu, J. Li, Y. Li, *J. Am. Chem. Soc.* **2017**, *139*, 7294–7301; c) F. Huang, Y. Deng, Y. Chen, X. Cai, M. Peng, Z. Jia, P. Ren, D. Xiao, X. Wen, N. Wang, H. Liu, D. Ma, *J. Am. Chem. Soc.* **2018**, *140*, 13142–13146; d) Y.

Cao, Z. Sui, Y. Zhu, X. Zhou, D. Chen, *ACS Catal.* **2017**, *7*, 7835 – 7846; e) X. Huang, Y. Xia, Y. Cao, X. Zheng, H. Pan, J. Zhu, C. Ma, H. Wang, J. Li, R. You, S. Wei, W. Huang, J. Lu, *Nano Res.* **2017**, *10*, 1302 – 1312.

[4] a) Y. Liu, X. Liu, Q. Feng, D. He, L. Zhang, C. Lian, R. Shen, G. Zhao, Y. Ji, D. Wang, G. Zhou, Y. Li, *Adv. Mater.* **2016**, *28*, 4747 – 4754; b) Y. Liu, J. Zhao, J. Feng, Y. He, Y. Du, D. Li, *J. Catal.* **2018**, *359*, 251 – 260; c) D.-M. Rao, S.-T. Zhang, C.-M. Li, Y.-D. Chen, M. Pu, H. Yan, M. Wei, *Dalton Trans.* **2018**, *47*, 4198 – 4208; d) C. Li, Y. Chen, S. Zhang, J. Zhou, F. Wang, S. He, M. Wei, D. G. Evans, X. Duan, *ChemCatChem* **2014**, *6*, 824 – 831; e) A. Han, J. Zhang, W. Sun, W. Chen, S. Zhang, Y. Han, Q. Feng, L. Zheng, L. Gu, C. Chen, Q. Peng, D. Wang, Y. Li, *Nat. Commun.* **2019**, *10*, 3787; f) Y. Pei, Z. Qi, T. W. Goh, L.-L. Wang, R. V. Maligal-Ganesh, H. L. MacMurdo, S. Zhang, C. Xiao, X. Li, F. Tao, D. D. Johnson, W. Huang, *J. Catal.* **2017**, *356*, 307 – 314; g) G. Vilé, D. Albani, M. Nachtegaal, Z. Chen, D. Dontsova, M. Antonietti, N. López, J. Pérez-Ramírez, *Angew. Chem. Int. Ed.* **2015**, *54*, 11265 – 11269; *Angew. Chem.* **2015**, *127*, 11417 – 11422.

[5] a) B. Yang, R. Burch, C. Hardacre, G. Headdock, P. Hu, *ACS Catal.* **2012**, *2*, 1027 – 1032; b) C. S. Spanjers, J. T. Held, M. J. Jones, D. D. Stanley, R. S. Sim, M. J. Janik, R. M. Rioux, *J. Catal.* **2014**, *316*, 164 – 173; c) C. S. Spanjers, R. S. Sim, N. P. Sturgis, B. Kabius, R. M. Rioux, *ACS Catal.* **2015**, *5*, 3304 – 3315.

[6] Y. Chen, J. Chen, *Appl. Surf. Sci.* **2016**, *387*, 16 – 27.

[7] a) Y. Cao, W. Fu, Z. Sui, X. Duan, D. Chen, X. Zhou, *Ind. Eng. Chem. Res.* **2019**, *58*, 1888 – 1895; b) S. K. Kim, C. Kim, J. H. Lee, J. Kim, H. Lee, S. H. Moon, *J. Catal.* **2013**, *306*, 146 – 154; c) A. E. Yarulin, R. M. Crespo-Quesada, E. V. Egorova, L. L. Kiwi-Minsker, *Kinet. Catal.* **2012**, *53*, 253 – 261.

[8] R. Ducher, R. Kainuma, K. Ishida, *Intermetallics* **2007**, *15*, 148 – 153.

[9] Z. W. Ulissi, M. T. Tang, J. Xiao, X. Liu, D. A. Torelli, M. Karamad, K. Cummins, C. Hahn, N. S. Lewis, T. F. Jaramillo, K. Chan, J. K. Nørskov, *ACS Catal.* **2017**, *7*, 6600 – 6608.

[10] G. X. Pei, X. Y. Liu, A. Wang, Y. Su, L. Li, T. Zhang, *Appl. Catal. A* **2017**, *545*, 90 – 96.

[11] a) C. Li, M. Wei, D. G. Evans, X. Duan, *Small* **2014**, *10*, 4469 – 4486; b) A. Ota, M. Armbrüster, M. Behrens, D. Rosenthal, M. Friedrich, I. Kasatkin, F. Girgsdies, W. Zhang, R. Wagner, R. Schlögl, *J. Phys. Chem. C* **2011**, *115*, 1368 – 1374; c) A. Ota, J. Kröhnert, G. Weinberg, I. Kasatkin, E. L. Kunkes, D. Ferri, F. Girgsdies, N. Hamilton, M. Armbrüster, R. Schlögl, M. Behrens, *ACS Catal.* **2014**, *4*, 2048 – 2059.

[12] a) J. J. Rehr, R. C. Albers, *Rev. Mod. Phys.* **2000**, *72*, 621 – 654; b) A. I. Frenkel, A. Yevick, C. Cooper, R. Vasic, *Annu. Rev. Anal. Chem.* **2011**, *4*, 23 – 39; c) A. I. Frenkel, *Chem. Soc. Rev.* **2012**, *41*, 8163 – 8178; d) J. E. Penner-Hahn, *Coord. Chem. Rev.* **1999**, *190 – 192*, 1101 – 1123; e) Z. Sun, Q. Liu, T. Yao, W. Yan, S. Wei, *Sci. China Mater.* **2015**, *58*, 313 – 341.

[13] a) G. X. Pei, X. Y. Liu, A. Wang, A. F. Lee, M. A. Isaacs, L. Li, X. Pan, X. Yang, X. Wang, Z. Tai, K. Wilson, T. Zhang, *ACS Catal.* **2015**, *5*, 3717 – 3725; b) W. G. Menezes, L. Altmann, V. Zielasek, K. Thiel, M. Bäumer, *J. Catal.* **2013**, *300*, 125 – 135; c) G. X. Pei, X. Y. Liu, A. Wang, L. Li, Y. Huang, T. Zhang, J. W. Lee, B. W. L. Jang, C.-Y. Mou, *New J. Chem.* **2014**, *38*, 2043; d) L. Zhang, Y. Ding, K.-H. Wu, Y. Niu, J. Luo, X. Yang, B. Zhang, D. Su, *Nanoscale* **2017**, *9*, 14317 – 14321.

[14] J. Zhao, J. Xu, J. Xu, J. Ni, T. Zhang, X. Xu, X. Li, *ChemPlusChem* **2015**, *80*, 196 – 201.

[15] a) D. A. Torelli, S. A. Francis, J. C. Crompton, A. Javier, J. R. Thompson, B. S. Brunschwig, M. P. Soriaga, N. S. Lewis, *ACS Catal.* **2016**, *6*, 2100 – 2104; b) F. Studt, I. Sharafutdinov, F. Abild-Pedersen, C. F. Elkjær, J. S. Hummelshøj, S. Dahl, I. Chorkendorff, J. K. Nørskov, *Nat. Chem.* **2014**, *6*, 320 – 324.

Manuscript received: April 6, 2020
Accepted manuscript online: April 13, 2020
Version of record online: May 7, 2020

